Supporting Information

Bertrand et al. 10.1073/pnas.1208732109

SI Text

DNA Sequences and Self-Assembly. We describe here the oligo sequences used for the DNA nanotubes and DNA linker, and also describe details of linker assembly. The sequences of all oligos used are shown in Table S1. Fig. S1 depicts the assembly of nanotubes from tiles, while Fig. S2 shows the basic geometry of the tile–linker–tile assembly, showing all oligos and sequences.

Type-1 and type-2 nanotubes are self-assembled from tiles, which are themselves assembled from the "single-element" (SE) oligos (Fig. S1). Oligo sequences and assembly protocols are based on those used in ref. 1; see the *Materials and Methods* in the main text for assembly details. Both types utilize SE1, SE2, SE3, SE4, and SE5. Type-1 nanotubes carry a fluorescein amidite dye on SE3, and use SE6-1, while type-2 nanotubes carry a CY5 dye on SE3, and use SE6-2. In both cases, the six oligos form a tile with four sticky ends. These sticky ends mediate tile–tile binding, forming a curved tile sheet that closes on itself to form a tube. The SE6 oligos provide an additional 10 base overhang for attachment to the linker.

The linker is constructed from the plasmid pMal-p5×, which was transformed into chemocompetent TG1 bacteria via heat shock, then purified using a Maxi kit (Qiagen). The plasmid was then cut with the restriction enzyme AvaI and simultaneously dephosphorylated with Antarctic Phosphatase in a 2 h, 37 °C process containing 150 nM plasmid, 100 units of AvaI, 500 units of phosphatase, 20 mM Tris-acetate, 50 mM potassium acetate, 10 mM magnesium acetate, 1 mM DTT, 50 mM Bis-Tris-propane HCl, 1 mM $MgCl_2$, and 0.1 mM $ZnCl_2$. This resulted in four base overhangs CCGA and TCGG at either end. These overhangs were annealed and ligated to short double-stranded segments that are formed from the KFor and KRev oligos. Segment 1 was formed by annealing KFor-1 with KRev-1 (which have a 39 base complementarity), while segment 2 was formed by annealing KFor-2 with KRev-2 (also a 39 base complementarity). Annealing of the segments was carried out using 5 μM oligos in TE/NaCl buffer (10 mM Tris, 1 mM EDTA, 50 mM NaCl, pH 8) by ramping the temperature from 95 °C down to 4 °C over several hours.

Ligation of segment 1 to the plasmid's CCGA overhang and segment 2 to the TCGG overhang, was carried out using T4 DNA ligase in T4 DNA ligase buffer (NEB): first segment 1 (86 nM) and plasmid (130 nM) were mixed, and ligated in 1× ligase buffer containing six units of ligase at 4 °C for 15 h. Then segment 2 was added to the same concentration as segment 1, seven additional units of T4 ligase were added, and the mixture was incubated again under the same conditions. At the end of ligation, the mixture was purified using a Microcon YM-100 filter to remove excess protein and oligos, then resuspended in a Tris-Acetate-EDTA/Mg buffer.

Finally, to create biotin or digoxigenin labeled linkers, the KFor-1 oligo was modified by omitting the 10-base overhang (the first 10 bases listed in Table S1), adding the appropriate label to the 5′ end, then carrying through the annealing and ligation as before.

Note that, after assembly, both segment 1 and segment 2 carry the 3× FtsK orienting polar sequence (KOPS), GGGCAGGG–CAGGGCAGGG, oriented so the motor translocates towards the plasmid rather than towards the nanotube (2–4).

Gel formation occurred when linkers and nanotubes connect via the remaining 10 base overhangs–in particular, the overhang on KFor-1 is complementary to that on SE6-1, and the overhang on KFor-2 is complementary to that on SE6-2. The main text *Materials and Methods* describes the process of gel assembly.

Stiffening Due to Contraction of Linkers. We measure a roughly 10-fold increase in gel stiffness upon activation, whereas the absolute passive gel modulus is consistent with that of a network of entropic springs. Because FtsK is known to act on individual dsDNA strands, and not expected to appreciably change network topology, we attribute the stiffening of the gel to the increase in the spring constant of some fraction of the linkers while maintaining linker density. Here, we use a simple model to show that this effect can indeed replicate the observed stiffening using physically reasonable input parameters.

We base our model on two parallel nanotubes that are zippered together by multiple linkers. This geometry, sketched in the main text Fig. 1*A*, is expected because, once two nanotubes approach and become cross-linked by one linker, many other cross-linking sites on both nanotubes will be in close proximity and, thus, are highly likely to also form cross-links. We expect the key dimensions of the assembly to be set by the radius of gyration, $R_g \approx 150$ nm, of the linker. In particular, we take the linker spacing along the nanotubes to be $\approx R_g$ (because linker interpenetration would be entropically costly), and for the breadth of the double nanotube/linker assembly to be $\approx R_g$.

Given a total length L over which the nanotubes are zippered together, the number of cross-links will be L/R_g. We consider the elastic response of the system to a force, f, pulling the two nanotubes directly apart. We implicitly consider different geometries through different estimates of the contracted-linker spring constant; see below. We take a fraction ϕ of the linkers to be stably contracted by FtsK, and to elastically respond with a relatively stiff spring constant κ_1. The remaining fraction $1-\phi$ will be protein-free and respond with a relatively weak entropic spring constant $\kappa_2 \approx k_B T/R_g^2$. Assuming the nanotubes are perfectly rigid, the force required to separate the nanotubes by a distance δx is

$$f = \frac{L}{R_g}\delta x(\phi\kappa_1 + (1-\phi)\kappa_2) \qquad \textbf{[S1]}$$

Because the lateral dimensions of the system are $\approx R_g$, the stress is $\sigma = f/(LR_g)$, and the strain is $\varepsilon = \delta x/R_g$. The modulus is then found as $E(\phi) = \sigma/\varepsilon = f/(L\delta x)$. This gives a protein-free, passive modulus, $E(\phi=0) = \kappa_2/R_g \approx k_B T/R_g^3$, consistent with expectation. The experimental observation of a 10-fold stiffening corresponds to $E(\phi)/E(\phi=0) \approx 10$, resulting in the following constraint on the relative stiffness of the two types of linkers:

$$\frac{\kappa_1}{\kappa_2} = \frac{9}{\phi} + 1 \approx \frac{9}{\phi}. \qquad \textbf{[S2]}$$

Thus, the measured 10-fold stiffening upon activation can be explained by, e.g., 1% of the linkers ($\phi = 0.01$) becoming 1,000 × stiffer ($\kappa_1/\kappa_2 \approx 900$) upon contraction by the protein.

Such a large change in linker stiffness is reasonable because the initial entropic elasticity is very weak, whereas the lack of DNA contour means the final contracted state will have little entropic freedom, instead likely deriving its compliance from the enthalpic elasticity of the DNA and protein. An order-of-magnitude estimate for κ_1 can be derived by ignoring the presence of the bound protein, and estimating the bend and stretch compliance of a short rod of dsDNA. We consider both bend and stretch to account for the different possible deformation geometries in the gel. We estimate the length of the contracted linker to be ≈50 nm, because the protein and short remaining DNA contours

are all of order 10 nm in size. The measured stretch modulus of dsDNA is 1,000 pN (5), giving a spring constant for stretching of $1{,}000/50 = 20$ pN/nm. The spring constant for bending a rod is $\frac{3l_pT}{L^3} \approx 5 \times 10^{-3}$ pN/nm, using a persistence length $l_p \approx 50$ nm and a contour length $L = 50$ nm. The entropic spring constant $\kappa_2 = k_BT/(2R_g^2) \approx 10^{-4}$ pN/nm. This indicates the ratio κ_1/κ_2 will be between 10^2 and 10^5. This DNA-only estimate is likely a lower bound because the presence of a large bound protein is expected to increase the strand stiffness.

We conclude that the measured 10-fold increase in modulus is consistent with a network transformation in which a small fraction of the linkers become much stiffer (e.g., 1% of the linkers becoming 10^3 more stiff), and that a large increase in single-linker stiffness is physically reasonable.

1. O'Neill P, Rothemund PWK, Kumar A, Fygenson DK (2006) Sturdier DNA nanotubes via ligation. *Nano Lett* 6:1379–1383.
2. Bigot S, Saleh OA, Cornet F, Allemand JF, Barre FX (2006) Oriented loading of FtsK on KOPS. *Nat Struct Mol Biol* 13:1026–1028.
3. Ptacin JL, Nollmann M, Bustamante C, Cozzarelli NR (2006) Identification of the FtsK sequence-recognition domain. *Nat Struct Mol Biol* 13:1023–1025.
4. Bigot S, et al. (2005) KOPS: DNA motifs that control *E. coli* chromosome segregation by orienting the FtsK translocase. *EMBO J* 24:3770–3780.
5. Wang MD, Yin H, Landick R, Gelles J, Block SM (1997) Stretching DNA with optical tweezers. *Biophys J* 72:1335–1346.

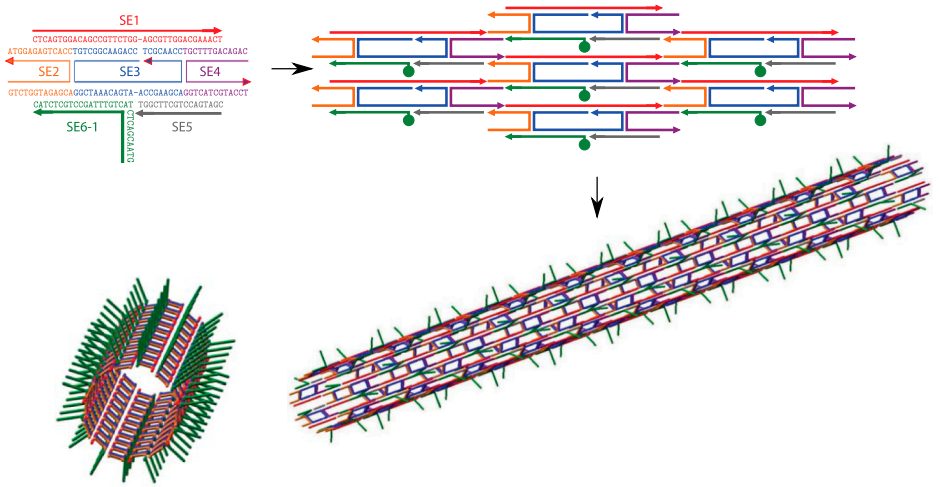

Fig. S1. Schematic of nanotube assembly: Individual tiles are formed from six SE oligos, then tiles associate to form a tube. The assembly of a type-1 nanotube is shown; type-2 nanotubes assemble identically, differing only in the sequence of the protruding ssDNA strand.

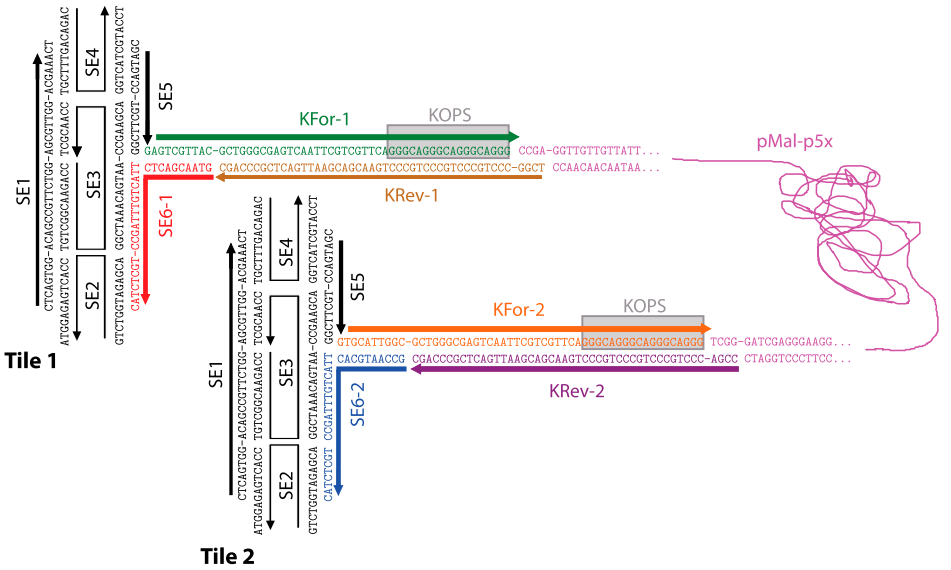

Fig. S2. Schematic of DNA gel self assembly. Tile 1 and tile 2 are individual elements from each type of nanotube; the full nanotubes are omitted for clarity. The nanotubes are linked to either end of a long plasmid, pMal-p5×, through short dsDNA segments formed from the KFor and KRev oligos. These segments contain the FtsK-orienting KOPS sequences.

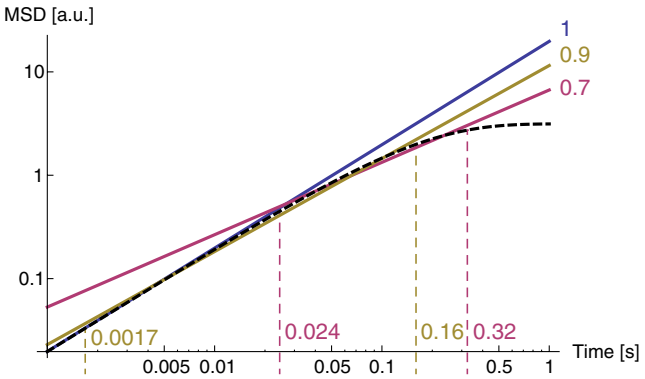

Fig. S3. Comparison of sublinear power-laws to mean-squared displacement (MSD) behavior in the vicinity of the plateau transition. The black dashed line represents an ideal model of the MSD for our system; it is generated analytically from a Lorentzian power-spectral density (PSD) with a 1 Hz shoulder (a good model for the measured PSDs in Fig. 4*B*). As shown, the ideal MSD asymptotically approaches linear behavior (blue line) at short times, and plateaus for times larger than 1 s. In our data, we only measure the MSD over a limited range and find best-fit power-laws with sublinear (exponents α between 0.7 and 0.9). Here, we show that these systematic underestimates, $\alpha < 1$, are likely due to the proximity of the plateau transition: We plot power-laws with $\alpha = 0.7$ (purple) and 0.9 (yellow) that closely follow the ideal MSD for over a decade in time. The vertical dashed lines indicate the range over which the respective power-law remains within 10% of the ideal MSD; as shown, this range is nearly two decades for $\alpha = 0.9$, and over a decade for $\alpha = 0.7$.

Table S1. Sequence of oligos used in nanotube assembly (SE oligos) and in linker attachment (KFor and KRev oligos)

oligo name	sequence
SE1	CTC AGT GGA CAG CCG TTC TGG AGC GTT GGA CGA AAC T
SE2	GTC TGG TAG AGC ACC ACT GAG AGG TA
SE3	CCA GAA CGG CTG TGG CTA AAC AGT AAC CGA AGC ACC AAC GCT
SE4	CAG ACA GTT TCG TGG TCA TCG TAC CT
SE5	CGA TGA CCT GCT TCG GT
SE6-1	GTA ACG ACT CTA CTG TTT AGC CTG CTC TAC
SE6-2	GCC AAT GCA CTA CTG TTT AGC CTG CTC TAC
KFor-1	GAG TCG TTA CGC TGG GCG AGT CAA TTC GTC GTT CAG GGC AGG GCA GGG CAG GG
KFor-2	GTG CAT TGG CGC TGG GCG AGT CAA TTC GTC GTT CAG GGC AGG GCA GGG CAG GG
KRev-1	TCG GCC CTG CCC TGC CCT GCC CTG AAC GAC GAA TTG ACT CGC CCA GC
KRev-2	CCG ACC CTG CCC TGC CCT GCC CTG AAC GAC GAA TTG ACT CGC CCA GC